*Article citation info:*
Siczek K, Woźniak M, Rylski A, Stachurski W. The effect of operating factors on the behavior of the combustion engine valve timing system. Combustion Engines. 0000;XXX(X):xx-xx. https://doi.org/10.19206/CE-204320

*Krzysztof SICZEK*
*Marek WOŹNIAK*
*Adam RYLSKI*
*Wojciech STACHURSKI*

**Combustion Engines**
Polish Scientific Society of Combustion Engines

# The effect of operating factors on the behavior of the combustion engine valve timing system

ARTICLE INFO

Received: 28 March 2025
Revised: 17 April 2025
Accepted: 23 April 2025
Available online: 5 May 2025

*Issues related to the various driving gears of the valve trains were discussed, along with the factors affecting them. The study was focused on the effect of disassembling the toothed pulley shrink-fitted to the crankshaft journal, followed by their assembly via pressure fitting. The roughness parameters for surfaces of a new and worn toothed pulley and worn crankshaft journal, as well as their hardness values, were measured. The model for calculations of friction coefficient, contact pressure, and friction torque carried by the contact zone was developed. It was found that the disassembling and assembling of the analyzed components can significantly weaken the interference between them. The weakening was accompanied by a decreased contact pressure. The plastic saturation occurred in the contact zone. The corresponding values of the friction coefficient were much higher than those for elastic stress in the contact zone. The friction coefficient values for the plastic saturation conditions differ from each other by up to 10%. Although all values of torque loading the worn toothed pulley exceed values of friction torque carried by the contact zone under plastic saturation, the displacement of the toothed pulley about the crankshaft journal can occur due to possible changes in the friction coefficient in the contact zone. The friction coefficient values can be lowered due to the presence of oxides, impurities, and engine oil droplets introduced into the contact zone by way of the oil mist present inside the engine block.*

Key words: *combustion engine, valve timing system, operating factors*



## 1. Introduction

Nowadays, each internal combustion engine (ICE) possesses valve timing that drives and controls the charge exchange process. Valve timing can be met in three arrangements [15]:

- Overhead Camshaft (OHC) Systems with camshafts placed directly above the valves, eliminating the need for pushrods. It is met in high-speed engines.
- Overhead Valve (OHV) Systems, also called pushrod systems, have the camshaft located inside the engine block and are comprised of pushrods to control the valves. They are used in heavy-duty engines that do not need high speeds.
- Double Overhead Camshaft (DOHC) Systems have two camshafts per row of cylinders: one for inlet valves and one for outlet valves, allowing the valves to be adjusted separately. Such systems provide better airflow at high engine speeds and produce more power due to less inertia than Single Overhead Camshaft (SOHC) systems.

Depending on its arrangement, a valve train can possess various components made of various materials and sometimes covered by protective layers [47], including valves, their seats, and guides [29] both in cam and camless valve trains. In cam valve trains and sometimes in camless, one-side valve trains occur valve springs sometimes mating with the valve rotators, keeping valves cleaner and reducing carbon build-up [28]. Only in cam valve trains can one meet rocker arms, push rods, tappets, and camshafts driven via chain or toothed belt gear, or seldom via gear from the engine crankshaft [47]. Camshafts are supported in bearings situated in the cylinder block or cylinder head, while rocker arms are supported in bearings mating with the axis fixed in the cylinder head. Bearings are lubricated by engine oil. Between the valve stem and the rocker arm or tappet, the hydraulic lash adjuster is placed to adjust valve lash [10, 76] automatically. Movable components of valve trains are often made of lightweight materials like, for example, Ti alloys to lower their inertia [60].

Jelenschi et al. [28] characterised five types of valve train, including the direct-acting OHC, the end pivot rocker arm OHC, the centre pivot rocker arm OHV, the centre pivot cam follower OHV, and the pushrod OHV. For the direct-acting OHC, Jelenschi et al. [27] reported that engine valve rotation is needed to lower the wear and the carbon deposits, improve the temperature distribution on its head, lower the risk of cracking and provide a better cylinder sealing. The major decrease in valve rotation appeared when the oil temperature was raised.

From the functionality point of view, the valvetrain is a series reliability structure, where the failure of one component causes the failure of the entire structure and serious disruptions in the engine operation. It may even result in its failure, as was the case with the engine analyzed in this article. Any flow disturbances in the engine oil system negatively affect the operation of engine components, including the timing system, especially by increasing the resistance to motion and wear of interacting components [48, 51, 62]. According to [8], a stable valve train operation strongly affects the engine efficiency. Further, the stability behaviour facilitates simulations of valve trains since instabilities are challenging for numerical solvers.

According to [59], valve timing, as well as valve lift and valve duration, allows for enhancing engine performance and optimizing fuel efficiency. Various variable valve control systems optimize power and torque by varying valve opening times and/or duration. This can be achieved via

various devices ranging from mechanical ones to hydraulic, pneumatic, electric ones, and camless systems [17].

The popular Variable Valve Timing (VVT) systems for various engines fall into two classifications: stepped and continuous. Stepped systems were utilized in older vehicles. They were restricted to just a handful of positions. Usually, there was an option for low engine speed and high speed, along with another for mid-range speed in some situations.

The majority of current VVT systems are categorized as continuous. The extent to which intake and exhaust valves can be opened (lift) and the length of time they can remain open are determined solely by the configuration and dimensions of the camshaft lobes and/or rocker arms (valve actuator) in this type of setup.

The volume of air and fuel permitted to flow in and out of the combustion chamber directly influences the level of horsepower that every cylinder can generate. Intake valves function by opening to permit air into the compression chamber, while exhaust valves open to enable air to exit. At lower engine speeds, optimal engine performance and fuel efficiency require less air. When engine speed rises, greater airflow is necessary for optimal engine performance. The variation in the volume of intake air needed at low engine speed compared to high engine speed is what justifies the use of the VVT system in automotive applications.

Any recorded failed VVT system code can lead to the deactivation of the complete VVT system. If this happens, there is an immediate and clear drop in engine performance and fuel efficiency.

The majority of contemporary VVT systems employ engine oil (hydraulic) pressure along with an electronic solenoid to trigger adjustments in valve timing, lift, and/or duration. A frequent issue encountered while diagnosing a malfunction in a VVT system is low engine oil level or low oil pressure. If there is not adequate engine oil pressure, the VVT system will not function as intended. Insufficient engine oil pressure can lead to severe engine damage while also negatively impacting the VVT system. The engine needs to have the appropriate oil filled to the correct level. If the oil pressure is uncertain, a manual oil pressure test might be necessary.

Certain VVT systems function with separate cylinder actuators, while others modify cylinders collectively. Others modify all the cylinders on a specific engine bank (simultaneously) using an oscillating camshaft. If the vehicle involved has one cylinder of the VVT system turned off, fuel efficiency and engine performance might slightly decrease. If the entire engine bank has the VVT system turned off, there will be a significant drop in fuel efficiency and engine performance. The specific kind of VVT system in an engine can significantly influence how much fuel efficiency and engine performance decline during a VVT malfunction.

Allowing an interference engine to lose timing is extremely hazardous when the valves and pistons are in the same location simultaneously. Interference is frequently linked to malfunctioning timing belts, tensioners, and water pumps, yet VVT actuators can also fail, leading to severe outcomes.

However, many internal ICEs still utilize valvetrains with a camshaft. According to [53], the connection from the crankshaft to the camshaft in an ICE is typically achieved through either a cogged belt transmission or a chain transmission when high mileage is needed without maintenance. The valvetrains in compression ignition (CI) engines occasionally utilize gear transmissions, and the traditional bevel gear can be seen in vintage collector cars or certain motorcycle engines. The chain gear utilized in spark ignition (SI) engines features a two- or three-row chain with high durability, owing to the irregular loads that also cause chain tension and valve timing disruption. The chain transmission necessitates the use of pre-tensioners, typically self-operating and powered by springs or hydraulic pressure. The vibrations and chain runout are restricted by employing plastic guides situated on the outer sides of the extended straight segments of the chain. The chain transmission model created using the Finite Elements Method and functioning under oil lubrication conditions was examined. This model facilitated the calculation of the weight and mass inertial moments of the components. The purpose of the research was to assess how the concentration of $SiO_2$ nanoparticles in engine oil influences the friction among chain transmission parts. The paper presents the resulting values of the friction torque in chain transmission functioning under various lubrication conditions.

Xin and Pinzon [68] reported that friction losses of the valve train can reach 7–15% of the engine total friction losses. The former can increase with a temperature increase. Dependent on the valve train design and engine speed, the friction increase is more or less significant [32].

Kamil et al. [30] reported that the valvetrain represents a major contributor to friction losses (up to 16%) within the engine across the complete engine speed spectrum. This is caused by the significant loads handled by the valvetrain across the full speed range. At reduced speeds, the valvetrain experiences loads mainly from spring forces, whereas at increased speeds, the inertia forces of the component masses take precedence. The cam follower connection accounts for the greatest friction loss because of the extremely high loads and small contact surfaces. Notably, greater losses take place at reduced speeds.

Irrespective of the drive type, a careful layout respecting design rules and optimization loops is needed for the best results in NVH, friction, and dynamic behaviour [20].

An interesting trend observed in modern ICEs is the use of camless valvetrains [50], like electrohydraulic ones.

Mitianiec and Bac [39] examined the management of ICE operations via a camless electro-hydraulic valve timing mechanism designed to reduce exhaust emissions and enhance overall efficiency. A simulation of an electro-hydraulic valve system was conducted in MATLAB–Simulink, varying the geometric parameters of the hydraulic system and the electric control parameters to achieve the desired valve lift and timing in the Toyota Yaris 1.3-liter gasoline engine. Furthermore, they analyzed engine parameters using a conventional cam valve system and a camless hydraulic valve timing system across various engine speeds. They observed a notable rise in engine torque and efficiency at elevated engine speeds for the examined camless system in the Toyota Yaris gasoline engine. SI ICEs featuring a camless unit drive exhibited improved perfor-

mance metrics compared to those with a traditional cam system. Improved valve lift characteristics over time led to an increased valve time-area and enhanced volumetric efficiency. The hydraulic valve drive system allowed for the regulation of the valve lift and reduced valve acceleration when compared to the cam system. The liquid feeding pressure in the system and the time for re-adjustment have the greatest impact on the valve lift trajectory. A hydraulic-driven valve timing system was more intricate and pricier compared to the traditional system.

Saleh and Chaichan [49] investigated how modifying the timing of the opening and closing of the inlet and outlet valves during the overlap period affects engine performance and exhaust gas emissions. The experiments were carried out on the experimental single-cylinder research engine of the SI engine type "Prodit." The variation in valve timings was achieved by adjusting the clearance distance between the rocker arm and the valve stem. Three valve overlaps (104˚, 108˚, and 112˚) were explored through theoretical and experimental methods. They discovered that minimizing the overlap period (overlap = 104˚) with an increased compression ratio (CR = 9) resulted in improved trade-offs between overall performance and exhaust emissions. They noted increases in the volumetric efficiency (12.58%) and the brake thermal efficiency (5.65%). The fuel usage decreased by 3%, while exhaust emissions dropped by approximately 4.45% for hydrocarbons and by 20.19% for carbon monoxide.

A Variable Valve Timing solenoid is formulated to manage the oil flow to the engine's camshaft, adjusting for engine speed, load, and performance requirements. The flexibility of VVT is most apparent in enhanced engine responsiveness, better fuel efficiency, and lower emissions [24].

Hunicz et al. [23] mentioned that homogeneous charge compression ignition (HCCI) is currently a prominent trend in the advancement of gasoline ICEs. They highlighted a design and implementation of a research engine featuring direct fuel injection along with the ability for HCCI combustion through internal gas recirculation and negative valve overlap (NVO).

Hunicz and Gęca [21] examined the effect of boost pressure on the combustion process and exhaust emissions in a controlled auto-ignition (CAI) engine. The tests were conducted using a single-cylinder engine equipped with a VVT and direct gasoline injection. To reach auto-ignition, the in-cylinder temperature was increased through the application of internal gas recirculation (EGR) achieved via the negative valve overlap (NVO) method. Fuel dilution achieved by raising intake pressure led to a significant decrease in nitrogen oxide emissions from the cylinder. Nonetheless, the use of boosting led to an excessive increase in auto-ignition timing and a rise in pressure rate rise (PRR) at elevated engine loads.

Hunicz and Gęca [22] examined a gasoline HCCI engine featuring internal gas recirculation to determine the possible range of valvetrain configurations and air excess coefficients that enable the achievement of HCCI combustion. They identified factors influencing the charge exchange process and the consequent in-cylinder temperature.

They clarified that additional energy must be provided to the working medium to achieve the temperature required for the mixture's self-ignition in the cylinder. This can be achieved through internal gas recirculation utilizing the method of negative valve overlap.

Although NVO enables HCCI combustion, this approach can only achieve engine operation under low to medium loads. Significant load dilution in the cylinder from internally recirculated gas and elevated temperature levels throughout the intake process result in a reduction of the filling coefficient. The upper limit of engine load is also influenced by the allowable rate of pressure increase within the cylinder.

The charge exchange process in HCCI operating with negative valve overlap differs significantly from that occurring in standard 4-stroke engines. In standard engines, during valve overlap, pressure readings in the cylinder, along with the intake and exhaust manifolds, strive to balance. The incomplete equilibrium arises solely from the inertia of the flowing medium and the vibrations of the fluid column in the intake and exhaust ducts. For an engine with internal gas recirculation, equilibrium is not present. The exhaust valve shuts several dozen degrees C.A. prior to TDC, and the intake valve opens after a suitable delay. Increased flow resistances associated with reduced valve lift and opening angles are offset by the opening of a throttle.

Valve timings serve as the primary mechanisms enabling volumetric efficiency and exhaust gas recirculation rates. Hence, recognizing charge transport mechanisms is a highly significant matter regarding the arrangement of the combustion process. The exhaust gas enthalpy gathered in the cylinder raises the temperature of the working medium upon the intake valve's closure, allowing for the self-ignition of the fuel-air mixture during the last phase of compression. The thermodynamic parameters of the gas that is recirculated internally influence the amount of air that enters the cylinder.

Throughout the complete achievable load range, there exists a balance between the thermodynamic conditions of the intake medium and the exhaust medium exiting the cylinder. The volumetric efficiency rate, exhaust gas temperature, and exhaust gas recirculation rate are interconnected, and the overall mass of charge in the cylinder varies within narrow limits. In valve system configurations that enable the engine to operate autonomously in HCCI mode (eliminating the need for spark discharge), the thermodynamic processes associated with charge exchange ensure that the compression temperature curve remains appropriate, irrespective of the excess air coefficient and volumetric efficiency rate.

Many problems with valve timing can arise relative to the use of research engines.

To decrease the costs of research engine tests, Cieslik et al. [11] successfully modified an existing research engine cylinder head in such a way as to implement an electronically controlled variable valve timing system of the intake system. They used the process of reverse engineering, together with design assumptions that finally allowed the construction of the assumed solution.

The authors discovered that:

1. To allow the engine to function in HCCI mode, a balance must be maintained between the volume of exhaust gas held in the cylinder, the temperature of the exhaust gas, and the quantity and temperature of the intake air.
2. The feasible operational range of the engine in HCCI mode is constrained by the temperature at the closure of the intake valve (the temperature varies within a narrow range).
3. The temperature at which the intake valve closes is determined by the energy equilibrium of the charge exchange process. To ensure a proper flow of the charge exchange, it is essential to choose suitable valve timings and valve lifts.

## 2. Causes of valve timing malfunctions

### 2.1. Various malfunctions met in valvetrains

Woźniak et al. [67] examined the engine valvetrain system functioning under inadequate oil lubrication circumstances resulting from a faulty installation of the gasket between the block and the head, and evaluated it. A model was created that includes a camshaft, bearings, tappet-valve-spring subassemblies, and a portion of the lubrication system. It was employed to assess the load bearings and the quantity of oil provided. The volumetric wear of the journals on the camshaft and the bearing covers were evaluated. In the projected engine operation, the wear rate and motion resistance were analyzed for scenarios involving the engine with proper and improper lubrication.

According to [42], the common issues related to camshafts include poor lubrication, bent or broken camshafts, worn camshaft lobes, incorrect camshaft timing, and camshaft sensor failure. According to [18], camshaft failure is typically ascribed to one (or more) of these reasons: inadequate lubrication, incorrect break-in procedures, reusing old or worn parts, mechanical interferences, and substandard hardware or hardware not tightened to specifications. Also, Wanjari and Parshiwanikar [65] reported that camshaft failures can be caused by material properties, engine speed, or load on the engine, lubricant properties, etc.

A fractured or cracked camshaft can be triggered by factors related to poor installation and maintenance [73].

Bassey et al. [3] studied a vehicle camshaft, considering the in-service failure it undergoes due to multi-translated, non-proportional loading conditions. They concluded that AISI 1020 Steel (Cold Rolled) could not be used for camshafts, while AISI 4130 Steel (annealed at 865°C), lighter than AISI 1020 Steel (Cold Rolled), was more appropriate. The best was Ti-5Al-2.5Sn Annealed (SS) due to its highest yield strength and the lowest density of the three materials studied.

Ma et al. [35] examined the shortcomings of assembled camshafts utilizing tube hydroforming (THF) technology. The signs of failure in the assembled camshaft primarily consisted of wear, scratches, damage, holes, pitting, and distortion on the tubular surface. During torsion, factors such as varying torsion force, angular torsion, and torsion speed led to significant wear on the tubular surface, altering the frictional properties (surface roughness) between the tube and the cam, resulting in sudden changes in shear stress and residual contact pressure. Additionally, relative movement happens between the tube and the cam, leading to the failure of the assembled camshafts.

Zhao et al. [74] studied the maximum contact stress in the shrink-fit camshaft assembly. They found that there is a maximal radial interference, below which there is no plastic deformation, and which can be used as the limitation for radial interference. For the mean diameter of the joint equal to 24 mm, the maximal radial interference was 0.08 mm. For the shrink-fit camshaft analyzed, the friction coefficient values' range was 0.14–0.19.

According to [66], a malfunctioning rocker arm results in the following symptoms:

- Tapping or clicking sound
- Decrease in engine power and efficiency
- Rough idling or stalling.

Although it is feasible to drive a short distance with a damaged rocker arm, doing so adds extra loads on the regular wear components of the valve train. Additionally, the faulty rocker arm can cause the engine to misfire.

Soffritti et al. [52] studied the factors contributing to wear at the rocker arm/pushrod and rocker arm/valve junctions of a diesel engine used in industrial cleaning machines, following just 1000 hours of engine use. The swapping of tappets for hydraulic valve lifters not only lowered the durability but also necessitated additional maintenance. The uneven wear damage appeared at the rocker arm/valve connection, caused by a misalignment of the valves about the valve seat inserts. In rocker arms and pushrods, inappropriate austenitization conditions and/or inadequate inductor design resulted in residual free ferrite, leading to failure to meet the necessary specifications for the induction hardening process. All surfaces showing wear were marked by material loss through scuffing; the onset of fatigue cracks was noted at the rocker arm/valve junction, and erosive cutting took place at the rocker arm/pushrod interface.

Yu and Xu [70] examined a malfunction in two diesel engine rocker arms used in trucks. The break happened at the bore of the rocker arm shaft in two instances. Beach marks and fatigue striations appeared on the fractured surface. Fatigue from multiple origins was the primary mechanism of failure.

According to [2], under high spring pressures, pushrods can deflect and throw off the valve timing. Also, according to [19], an incorrect pushrod length, whether too long or too short, can lead to issues ranging from reduced power to severe failure of one or multiple key valvetrain parts.

Morehouse et al. [40] examined the issues with diesel engine valves, which can be linked to the buildup of deposits on them. The influence of unburned and partially burned fuel on lubrication oil dilution is more significant in valve deposit formation than the oxidative stability of the oil itself. The upkeep (lubrication oil contamination), functioning (modifications of air intake, fuel delivery, and coolant circulation), part supply (manufacturing processes adverse impacts), and design (prime mover properly sized for the job to guarantee it operates within its efficiency range), are vital for valvetrain maintenance.

Raghuwanshi et al. [46] studied various failure modes of engine valves, failures due to fatigue at high temperatures, high-temperature effects on the mechanical properties of materials like hardness and yield strength, wear failure due to impact loading, and wear rate affected by load and time.

Vélez Godiño et al. [64] examined the failures detected in the valve train system of two distinct engine types, one powered by diesel and the other by compressed natural gas, associated with a fleet of city buses. The analyzed failure happened in over 20 distinct units, with the impacted components including both the cams (material loss at the cam tip) and the tappets (hard surface removal and significant tappet core deformation).

Yu and Xu [71] indicated that in a diesel engine of a truck, four valve springs for both intake and exhaust and two valves for both exhaust and intake were broken. The main failure mechanism for all four valve springs was fatigue fracture. A fatigue crack began in the spring wire of coil 1.3–1.5 at the upper end of the spring due to the maximum normal stress. This area is additionally the most affected site by contact friction wear. The fatigue fracture of the inlet and outlet valve stems was also caused by the malfunction of the related valve springs.

Patel and Pawar [44] documented the early fatigue failure of an exhaust valve spring in a constant speed C.I. engine. The failure of the spring resulted from inadequate fatigue life and reduced spring stiffness. Spring was durable enough for a 1500 rpm engine, but its lifespan diminished as the engine speed and inertia forces rose in a 2200 rpm engine. The pressure was more concentrated at the sight of failure. Additionally, a minor impact from elevated temperature, caused by increased engine speed, contributed to the failure of the spring.

Several studies have been conducted on problems with camshaft drive gears.

Howlett et al. [20] compared the main timing drive concepts, chain drive, dry belt, and wet belt based on the functional influencing factors like friction losses, wear modes, NHV, and other.

Li et al. [33] examined the failure mode of the roller chain while testing the timing chain in a minibus engine. The primary causes of the timing chain failure included the roller's fracture and fatigue debris on the roller surface, wear and corrosion on the sleeve interior, and oxidation and fretting wear on the pin. The timing chain system's wear and tear mechanisms included oxidation erosion, grooves, and fatigue deterioration. The defect beneath and the pressure on the edge of the roller step were the primary factors influencing the operational lifespan of the timing chain.

Yuan et al. [72] studied the fracture failure of a marine diesel engine timing gear. The fracture was of a fatigue nature, and the inclusions induced the initial cracks.

Lus [34] analyzed marine diesel engines using electronic control in valve gear mechanisms. The problems connected with the operation of valve gear mechanisms and their diagnostics were discussed. The diagnostic methods and processes affecting the diagnostic process were shown. Diagnostic methods based on vibration signal analysis are sensitive to engine load and speed changes, but allow validating the state of engine components, such as its valve train.

The VVT system can affect the valve timing via a phase shifter located at the head of the camshaft. This part is activated by the engine control unit using oil flow controlled by the solenoid valve [16].

According to [24], VVT solenoid malfunction can be induced by:

1. Contamination: Lengthened oil change intervals may result in the buildup of contaminants like dirt, debris, and other solids in the engine oil. This can accumulate in the oil channels of the VVT system, leading to issues that vary from solenoid malfunction to early wear of the chain and gears caused by insufficient oil lubrication.
2. Electrical problems: Issues like wiring damage or inadequate connections can interfere with the communication between the Engine Control Module (ECM) and the VVT solenoid, leading to improper functioning.
3. Engine overheating: Prolonged exposure to elevated temperatures can lead to the deterioration of solenoid components. High temperatures can lead to oil degradation (insufficient lubrication) and unpredictable performance in the electrical system.
4. Wear and tear: The VVT is a mechanical part. Routine oil changes prolong VVT functionality, but standard wear and tear will ultimately degrade parts in the VVT system.

Typical signs of the VVT solenoid malfunctions are as follows.

1. Malfunction Indicator Lamp (MIL) or Check Engine Light (CEL) is turned on – if the VVT solenoid fails to operate, the ECM may activate the MIL or CEL to light up on the vehicle's dashboard. This will include a Diagnostic Trouble Code (DTC), an explanation, and related Freeze Frame Data.
2. Decreased Engine Performance – the main role of the VVT Solenoid is to control the camshaft timing, guaranteeing seamless engine operation under different conditions. The failure of the VVT solenoid may lead to decreased power, acceleration, and fuel efficiency.
3. Unusual Sounds from the Engine – if the VVT solenoid malfunctions, it fails to modify the valve timing correctly, resulting in inconsistent valve movements and possible clashes between parts. Moreover, if the VVT system functions incorrectly, it may cause heightened vibration and resonance in the engine, resulting in unusual sounds.

It can be found that most reported studies on failed components of cam-based valvetrains related to valves, their seat inserts, and valve springs. No studies related to the failure of camless valvetrains have been found in the literature.

### 2.2. Failures of the valvetrain driven by a toothed belt

Domek et al. [13] examined the quality of timing belt pulleys, which greatly affects the coupling of the timing belt with the pulley due to issues related to movement and displacement accuracy. The latter relies on the quality of the belt gears and, in particular, the quality of the pulley. Measurements of these reveal various errors, impacting the kinematics and dynamics of the entire transport system. It is

also among the key factors affecting the longevity of the timing belt. The quality of the wheels is also influenced by the selected production method, which relates to the material and the capabilities of the manufacturer.

Domek et al. [14] analyzed the course of volumetric wear of timing pulleys depending on the properties of the belt-pulley friction pair.

According to [63], a timing belt, often referred to as a cam belt, is a crucial component of numerous engines. It is a robust yet adaptable strip composed of rubber, polyurethane, and neoprene, strengthened with cords, which links the crankshaft to the camshaft or camshafts. The timing belt coordinates the elements inside the engine to guarantee they function together smoothly.

The design of a timing belt typically includes two layers of rubber encasing nylon fibers, polyester cords, or steel wires. These materials provide the belt with the flexibility and strength needed to endure significant tension and vibration while it rotates shafts at varying speeds for long durations. It features internal teeth that connect with the cogs on the crankshaft and camshaft gears, while the belt's outer surface is flat.

A timing belt primarily ensures that all moving parts, such as the pistons and valves, remain properly aligned – or synchronized – during operation. This stops any impacts from happening within your engine that could cause significant harm. Furthermore, the timing belt guarantees that the valves open and shut at the appropriate times for their associated cylinders to receive air or fuel, allowing combustion to be effectively regulated for optimal performance.

Ultimately, a timing belt aids in lowering emissions by enabling slight modifications to the combustion process, particularly in engines equipped with variable timing features, leading to more efficient and cleaner engine performance.

If the timing belt skips teeth on a gear or breaks, the effects can range from minor to severe, depending on the extent of the problem and the engine design. It might involve just changing the belt, or it could be a severe engine failure that needs an engine rebuild or replacement.

A malfunctioning timing belt can lead to significant harm to the engine.

A frequent reason for timing belt failure is the age of the belt. The substances used to create a belt will ultimately dry out and become fragile because of the hot, arid working environment, which weakens the belt and leads to fractures. Timing belts have their manufacturing date marked on them. The timing belt is regarded as a service part that needs to be replaced at regular intervals [63].

Noticing other indications of a degraded belt can prevent expensive repairs later. Such indications comprise:

– Noticeable wear and tear are the most reliable indicator of a used timing belt. This may involve fraying, cracking, stretching, or noticeable loss of material. Inspecting the timing belt is often challenging, however, due to the considerable work required to reach it.
– Loud engine noise is another indication that your timing belt may require replacement. A belt that has missing teeth or is excessively stretched can no longer keep the timing, resulting in loud clacking and rattling sounds when you start your vehicle. Eventually, these noises might become so loud that they can be heard even while driving at slow speeds.
– A generally reduced performance suggests that there is an issue with the car's timing belt. The vehicle might face reduced acceleration performance or have difficulty sustaining speeds over specific thresholds, and the issue could be an aged or defective belt.
– A Check Engine Light frequently activates with DTCs associated with the camshaft position or crankshaft position sensors. Often, the engine will experience misfires and display DTCs ranging from P0300 to P0308.
– A tapping or slapping noise within the engine may also signify a faulty timing belt. Belt segments may tear and, while remaining attached, strike the inner side of the covers covering the timing belt.
– An engine that cranks over too easily but fails to start indicates that the timing belt has completely snapped. Referred to as freewheeling, the starter rotates the crankshaft but no longer engages the camshaft since it’s disconnected.

It’s essential to identify the additional indicators of a faulty timing belt before this symptom appears to avoid causing more damage. One might not exhibit any noticeable symptoms before the belt failure, which is why regular maintenance is crucial for the timing belt. The service manual for vehicles includes the suggested interval for replacements, typically between 60,000 and 100,000 miles.

According to [12], timing belts can malfunction and create serious issues if not dealt with promptly. The causes of such malfunctions comprise:

– Excessive load – it is a contributing factor to the failure of the timing belt. If the teeth of the timing belt are breaking, the main reason is an excessive load. Over time, pulleys may encounter misalignment and bearing wear that can create excessive strain on the belt. You must consistently check the Optibelt Omega HI and, in addition to consulting a manufacturer, avoid any issues to safeguard your timing belt.
– Insufficient maintenance – it is a further cause of timing belt failure. The health of every vehicle component, including timing belts, must be preserved. It is essential to recognize the initial indications of deterioration, such as fraying, glazing, and cracking, which may lead to failure. Routine maintenance is essential, as neglecting belt tension adjustments or oil leaks may escalate stress on the timing belt, heightening the risk of failure.
– Debris and pollutants – their appearance on a timing belt may indicate a potential failure. When external particles build up on the surface of the belt or within the belt tensioner, it may impair the belt's flexibility and hinder its smooth performance. Numerous factors can hinder a belt's flexibility, including dirt, dust, oil spills, and others that may lead to belt deterioration and breakdown. Make sure to examine and assess feasible actions to avert the problems frequently.
– Overheating – the action of any part can affect the durability of a timing belt. In this case, the timing belt is no different. Elevated temperatures can lead to the deterioration of timing belt materials, resulting in cracks and

other issues. The engines can overheat because of faulty cooling systems or insufficient coolant levels, which can speed up the process. Guarantee appropriate upkeep to tackle the indications of overheating.

- In case of too loose tension, the belt may slip and skip teeth, causing engine timing misalignment. Excessive tension can speed up wear and strain on the belt, causing premature failure [7].
- Oil leaks present a serious risk to timing belts. When oil interacts with the rubber, it leads to the degradation of the belt. Moreover, oil serves as a lubricant. It minimizes the friction needed for the belt to hold onto the pulleys. This slick scenario may cause the belt to slip and malfunction [7].

The outcomes of a timing belt breakdown comprise [63]:

- Certain engines are classified as interference-type engines. If the timing belt snaps, these engines may suffer severe damage to internal parts due to the risk of pistons hitting the valves. In non-interference engines, the chance of internal engine damage is lower, yet in either case, the engine will halt instantly. The expenses are high to fix this issue are high, and since it frequently occurs while navigating through traffic, it can also represent a significant safety hazard.
- A broken timing belt may lead to oil leaks. A notable change in the pressure within an engine can create stress on various parts, like seals or oil pan gaskets. This unnecessary pressure frequently leads to these components breaking or becoming worn, causing oil leaks in the surrounding area. It might increase the repair cost.
- Even if the belt elongates or misses, damage may result. It may lead to issues with the fuel injectors, cause subpar performance, and result in a misfire, making your vehicle unreliable to operate until it is repaired. Certain issues will be fixed by simply replacing the belt, whereas others may need costly components to be changed along with the timing belt.

To reduce the chances of belt failure, the subsequent actions should be taken [12]:

- Make sure to adhere to the replacement schedules suggested by the manufacturer, comprising the time and distance determined to be the safe limit for a timing belt's operation
- Make sure the engine compartment is free from any debris
- Keep the cooling system operating correctly and watch the coolant levels
- Perform routine oil changes to reduce engine friction and lower other systems' stress
- Seek advice from a qualified mechanic for any issues
- Maintaining the correct tension in a timing belt is crucial for its proper functioning. Regular checks and adjustments can extend the life of the timing belt by ensuring proper tension [7].

Domek et al. [13] examined the quality of timing belt pulleys, which greatly affects the coupling of the timing belt with the pulley due to issues related to movement and displacement accuracy. The latter relies on the quality of the belt gears and, in particular, the quality of the pulley. Measurements of these reveal various errors, impacting the kinematics and dynamics of the entire transport system. It is also among the key factors affecting the longevity of the timing belt. The quality of the wheels is also influenced by the selected production method, which relates to the material and the capabilities of the manufacturer.

Domek et al. [14] analyzed the course of volumetric wear of timing pulleys depending on the properties of the belt-pulley friction pair.

## 3. Methods and materials

### 3.1. Characteristics of the analyzed engine

The analysis was conducted for elements of DOHC ICE applied in KIA CeeD 1.4 EX (man. 5) manufactured in 2008, the model with 5-door hatchback body [1]. This naturally aspirated petrol engine possessed 4 cylinders in line. Its displacement was 1396 $cm^3$. It utilized CVVT (continuous variable valve timing) and electronic multi-point petrol injection. It reached the maximum power of 80 kW at 6200 rpm and the maximum torque of 137 Nm at 5000 rpm. Its main characteristics are shown in Fig. 1. It was assumed that the camshaft friction torque $M_c$ reaches its maximum value $M_{cmax}$ of about 60 Nm for 350 rpm, similarly to [9]. However, the camshaft friction torque lowered to about $0.8M_{cmax}$ for the camshaft speed of 750 rpm and to $0.5M_{cmav}$ for camshaft speed of 2500 rpm [9]. Considering the gear ratio of the toothed belt transmission u = 2, the torque $M_h$ loading the toothed pulley can reach up to 96 Nm for the engine crankshaft speed of 1500 rpm and 60 Nm for 5000 rpm. Reaching 96 Nm by the torque $M_h$ for the engine speed of 1500 rpm seems to be problematic due to engine characteristics (Fig. 1). However, fluctuations in engine speed can allow the development of this value if the vehicle's clutch is disconnected from the engine.

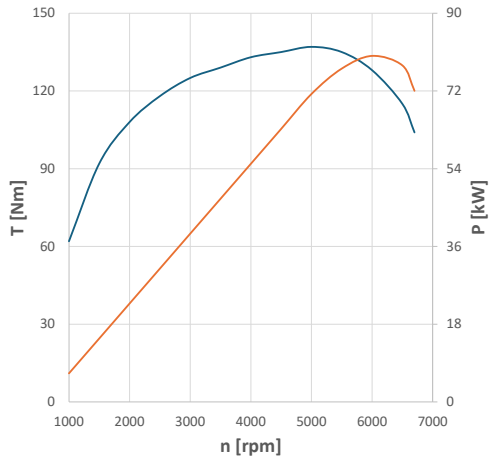


Fig. 1. Characteristics including power vs. speed and torque vs. speed for the SI engine applied in KIA CeeD 1.4 EX (man. 5) automobile manufactured in 2008, the model with a 5-door hatchback body (based on [1])

### 3.2. Failed tooted gear and crankshaft

The scheme of the toothed belt drive of the engine cam valvetrain is shown in Fig. 2a. This type of transmission contains a toothed belt mounted on toothed pulleys, a tensioner, and two guided dampers of belt vibrations. The crankshaft journal 1 mating with a toothed pulley 2 is presented in Fig. 2b. The crankshaft with a flywheel used in the analyzed ICE is shown in Fig. 2c. The surface of the

crankshaft journal mating with the toothed pulley analyzed is presented in Fig. 2d.

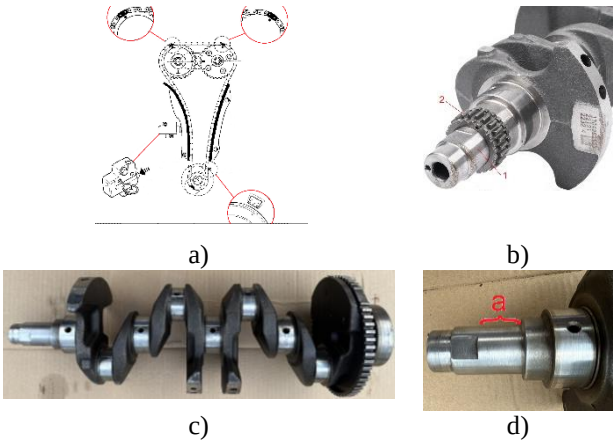


Fig. 2. The crankshaft of the analyzed ICE. a) scheme of the toothed belt drive of the engine cam valvetrain, b) the crankshaft journal 1 mating with toothed pulley 2, c) general view of the analyzed crankshaft, d) the crankshaft journal surface mating with toothed pulley bore at length "a"

### 3.3. The friction torque carried by the contact zone between the toothed pulley and the crankshaft journal

The friction torque carried by the contact zone between the toothed pulley and the crankshaft journal can be estimated from the formula (1) [5]

$$M = 0.5\pi d_w^2 L \mu p_s \tag{1}$$

where: $d_w$ – outer diameter of the crankshaft journal, L = 15 mm – length of the toothed pulley bore, μ – the friction coefficient in the contact zone between the crankshaft journal and the toothed pulley bore, $p_s$ – contact pressure in the contact zone between the crankshaft journal and the toothed pulley bore.

### 3.4. The friction coefficient in the contact zone between the toothed pulley and the crankshaft journal

Mendeleev [38] obtained empirical relations between the roughness parameters $R_a$, $R_{tm}$, $R_p$, $R_v$, $R_m$, S and the parameter $R_q$ for metal and ceramic surfaces produced by grinding, finishing, rolling, and sandblasting.

Booker and Truman [5] noted that a complicated mix of factors determines the static coefficient of friction, which makes it challenging to ascertain an exact value. Every variable influences this coefficient, especially those related to the surface roughness's interface pressure and loading direction. Numerous combinations of materials and processing methods can be utilized to produce feasible shrink-fit assemblies, impacting the values and variability of this coefficient. The values of such a coefficient, obtained through systematic experimentation, should be carried out on statistically significant sample sizes in a cost-effective manner to enable proper characterization of the friction coefficient variation.

Stamenkovic et al. [54] reported that the strength of different joints under heavy loads, like press-fit joints, is influenced by the static friction force. The actual value of the friction coefficient can be determined using the established calculation method derived from the molecular-mechanical friction theory. This process considered roughness metrics and the hardness of contact surfaces, along with the correlation between the deformation aspect of the static friction coefficient and the overall static friction coefficient measured in experimental conditions specific to tribology. The researchers examined tribological factors associated with the press fit connections of drive unit components in railway vehicles.

Ivković et al. [25] reported that the roughness parameters of the contact surfaces directly affect the coefficient of static friction. The latter grows with the parameters of surface roughness. However, there can be variations in static friction coefficient values within the same roughness category due to the method by which the surface is processed. The complex parameter of microgeometry can effectively represent this variation.

The friction coefficient can be determined by the formula [54]

$$\mu = k\Delta_K^{0.5}\left(\frac{p_c}{HB}\right)^{0.25} \tag{1}$$

where: $p_c$ – contour pressure [MPa] in the contact zone, HB – the Brinell hardness [MPa] of the softer material in contact zone, $\Delta_K$ – the Kombalov complex roughness parameter [-], k – the coefficient [-] that depends on the type of machining, the roughness of contact surfaces and correlation of surface hardness of assembled parts, the value of the surface pressure, as well as the lubricant.

According to [31], for plastic-saturated contact, the friction coefficient can be determined by the eq.

$$\mu = 0.1\frac{\tau_0}{HB} + \beta + 0.9\Delta_K^{0.5}\left(\frac{p_c}{HB}\right)^{0.5} \tag{2}$$

where: $\tau_0$ = 1256 MPa – the tangential shearing strength of the adhesion bond for plastic contact on rough steel surfaces, β = 0.072 – the pressure coefficient of the molecular component of friction characterizing the increase of shearing strength at normal pressure.

The Kombalov complex roughness parameter $\Delta_K$ can be determined by the formula [54]

$$\Delta_K = \frac{R_v}{r b^{1/\nu}} \tag{3}$$

where: $R_v$ – maximum roughness depth [μm], r – mean roughness asperity radius [μm], b, ν – constants [-], values of which depend on the distribution of the material in the rough surface layer. They can be determined experimentally. The value of the constant b ranges within 2 to 4, while that of the ν n is between 1.5 and 3. If the values of the roughness parameters $R_v$, $R_a$ and $R_p$ are known, then the values of the constants ν and b can be calculated from the formulas [54], respectively

$$\nu = 2t_m\frac{R_p}{R_a} - 1 \tag{4}$$

$$b = t_m\left(\frac{R_v}{R_p}\right)^{\nu} \tag{5}$$

where: $t_m$ – the relative reference length of the roughness profile at the level of the center line – it was estimated that $t_m \approx 0.5$, $R_p$ – maximum roughness peak height [μm], $R_a$ – roughness average [μm].

The mean roughness asperity radius r was determined from the formula [41]

$$r = \frac{9R_a^2 S_m^2}{128\left(5.5R_a - R_p\right)^3} \tag{6}$$

where: $S_m$ – mean spacing at mean line.

During the analysis of the friction in the contact zone between the crankshaft journal and toothed pulley bore, the equivalent roughness parameters are used. The equivalent roughness parameters were estimated from the formulas (7)–(11) [43], respectively. The subscripts: eqrelate to equivalent, s – relates to crankshaft journal, and h – relates to toothed pulley hub bore, respectively

$$R_{aeq} = R_{as} + R_{ah} \tag{7}$$

$$R_{zeq} = R_{zs} + R_{zh} \tag{8}$$

$$R_{veq} = R_{vs} + R_{vh} \tag{9}$$

$$R_{peq} = R_{ps} + R_{ph} \tag{10}$$

$$S_{meq} = S_{ms} + S_{mh} \tag{11}$$

The equivalent constant $t_{eq}$ was estimated from the formula [43]

$$t_{eq} = t_s + t_h \tag{12}$$

The equivalent constant $\nu_{eq}$ was estimated from the formula [43]

$$\nu_{eq} = \nu_s + \nu_h \tag{13}$$

The equivalent constant b was determined from the formula [54]

$$b_{eq} = t_{meq}\left(\frac{R_{veq}}{R_{peq}}\right)^{\nu_{eq}} \tag{14}$$

The equivalent asperity radius $r_{eq}$ was estimated from the formula [41]

$$r_{eq} = \frac{9R_{aeq}^2 S_{meq}^2}{128\left(5.5R_{aeq} - R_{peq}\right)^3} \tag{15}$$

The equivalent Kombalov complex roughness parameter $\Delta_{Keq}$ was determined by the formula [54]

$$\Delta_{Keq} = \frac{R_{veq}}{r_{eq} b_{eq}^{1/\nu_{eq}}} \tag{16}$$

As the ratio of the mean spacing at the mean line to mean roughness $S_m/R_a$ can vary in the range 250–2800 for smooth surfaces [26], it seems reasonable to assume the value of such a ratio equal to 1000 during analysis.

For the simplicity it was estimated that for grinded journals there is: $R_{veq}/R_{peq} \approx 1.2$ and $R_{peq}/R_{zeq} \approx 0.5$.

The coefficient k value can be experimentally determined for tribological conditions corresponding to maintenance conditions. Such a coefficient is dependent on the penetration depth h, whose dependence can be determined experimentally as shown in Fig. 3.

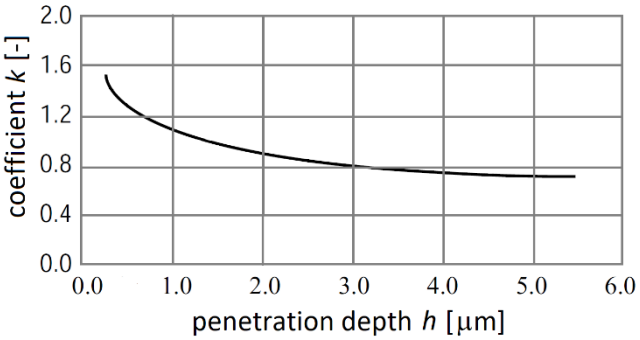


Fig. 3. The dependence between the coefficient k and the penetration depth h (based on [54])

The penetration depth h can be estimated from eq.

$$h \approx 3.4R_{aeq}\left(\frac{p_c}{HB}\right)^{1/3} \tag{16}$$

### 3.5. The hardness and the roughness of mating surfaces

The hardness of the crankshaft journal surface, mating with the belt transmission toothed pulley, was measured using the HRC hardness tester. The hardness of the bore surface of such a toothed pulley was assumed to be close to that on the side surface of the wheel measured near its bore (to avoid any influence of the surface hardening of the teeth on the hardness of the bore surface).

The roughness parameters of the crankshaft journal surface mating with the belt transmission toothed pulley were obtained using the Hommel Tester T8000 stationary contact profilometer (Hommelwerke GmbH, Schwenningen, Germany) with Turbo Wave V7.36 and Hommel Map 4.0 software. A measuring range of ±300 μm characterized such a measuring unit with a resolution of 1 nm across the entire range. Due to the limited accessibility of the profilometer measuring needle to the surface of the analyzed journal, it was necessary to cut out the section containing the analyzed journal from the crankshaft (Fig. 4a). Roughness measurement was carried out parallel to the axis of the tested crankshaft journal for eight cross-sections evenly distributed in a circularly symmetrical manner concerning the crankshaft journal. Eight measurement locations were determined at 45° intervals around the journal circumference, marked in Fig. 4b with symbols M1 to M8 (Fig. 4).

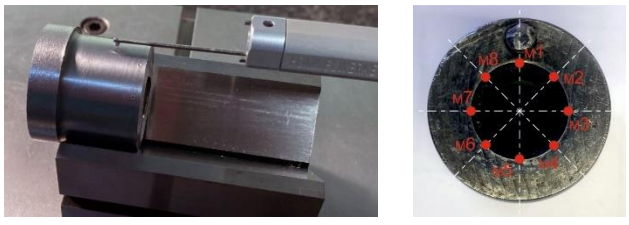


a) b)

Fig. 4. The measurement of the roughness parameters for the crankshaft journal. a) the partial view of the measuring stand with cut crankshaft section with the journal analyzed, b) the distribution of measurements around the circumference of the crankshaft journal

In the case of the bore surface of such a toothed pulley, the roughness parameters were obtained using the same profilometer (Fig. 5). On the profilometer measuring table,

1 was fixed, a measuring holder 2 with the tested toothed pulley 3. The measured profile was obtained via a measuring needle covered by holder 4 linked to the profilometer measuring head 5. Roughness measurement was carried out parallel to the axis of the tested toothed pulley 3 for eight cross-sections evenly distributed in a circularly symmetrical manner concerning the wheel bore, marked in Fig. 4 with symbols M1 to M8 (Fig. 6).


Fig. 5. The measurement of the roughness parameters for the bore surface of a toothed pulley using the measuring unit Hommel-Etamic W40. 1 – profilometer measuring table, 2 – measuring holder, 3 – tested toothed pulley, 4 – profilometer measuring needle holder, 5 – profilometer measuring head

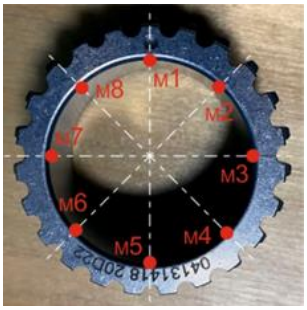


Fig. 6. The distribution of measurements around the circumference of the toothed pulley bore

### 3.3. The contact pressure in the interface between the toothed pulley and the crankshaft journal

The contact pressure in the interface between the toothed pulley and the crankshaft journal can be determined using the model shown in Fig. 7 [36].

Such a contact pressure can be determined from the formula [36]

$$p_s = E\Delta \frac{(d_w^2 - d_{ww}^2)(d_{zo}^2 - d_w^2)}{d_w^3(d_{zo}^2 - d_{ww}^2)} \quad (17)$$

where: E = 210,000 MPa – Young's modulus for the steel, $\Delta = \Delta d_o - \Delta d_w$ (Fig. 7), $d_w$ = 30 mm – outer diameter of the crankshaft journal, $d_{ww}$ = 12 mm – inner diameter of the crankshaft journal, $d_{zo}$ = 35 mm – outer diameter of the toothed pulley hub.

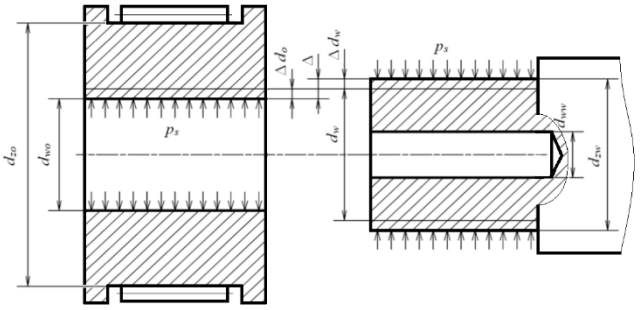


Fig. 7. The model for determining the contact pressure in the interface between the toothed pulley and the crankshaft journal

The toothed pulley was first shrink-fitted onto the crankshaft journal, then removed with a puller and put back on the journal with a press. This caused the roughness asperities of the journal and the toothed pulley bore to be cut off at least twice, weakening the interference between the toothed pulley and the journal. Therefore, the formula (17) should consider changes in the surface roughness of joined elements [37]. The modification assumes reducing the size of parameter $\Delta$ by the smoothing G dimension factor according to the formula [37]

$$G_i = 0.8(R_{zsi} + R_{zhi}) \quad (18)$$

where: $G_i$ – smoothing dimension factor after the i-th displacement of the toothed pulley bore surface on the crankshaft journal surface along the journal axis during their i-th assembling or disassembling, $R_{zsi}$ – corresponding roughness parameter $R_z$ of the crankshaft journal, before the i-th assemly or disasembly, $R_{zhi}$ – corresponding roughness parameter $R_z$ of the toothed pulley hub bore, before the i-th assembly or disassembly, $i = 2$ – number of assemblies or disassemblies during the engine operation.

Formula (17) takes the form [37].

$$p_s = E\left(\Delta - \sum_{i=1}^{i=2} G_i\right) \frac{(d_w^2 - d_{ww}^2)(d_{zo}^2 - d_w^2)}{d_w^3(d_{zo}^2 - d_{ww}^2)} \quad (19)$$

It was assumed that the shrink-fitted joint of the toothed pulley bore with the crankshaft journal was realized as the ∅30H7/u6. For this, values of the interference $\Delta$ range from 27 to 61 μm. The initial values of roughness parameters $R_{as}$ was 0.8 μm. This corresponds to the roughness parameter $R_{zs}$ value equal to 4.8 μm.

## 4. Results and discussion

### 4.1. Hardness and roughness

The measured hardness values for the toothed pulley front plane were equal to 42 HRC±0.5, which corresponds to 388 HB, and for the crankshaft journal, 24.5 ±0.5 HRC, which corresponds to 245 HB [55]. This was surprising, as the journal hardness is often higher than that of a gear hub tightly fitted to the journal. Additionally, according to [45], depending on the type and manufacturer of the engine, the crankshaft's hardness generally needs to be below roughly 450 HB. In critical zones where stress levels are elevated, like near the oil bore and fillets, a hardness limit of approximately 350 HB is typically required. If the crankshaft's hardness increases after a bearing failure, then in-situ heat treatment (annealing) could be the sole method to preserve

the crankshaft. The above-mentioned facts and observations may suggest that the surface of the tested journal in the analyzed crankshaft was not hardened or was under-hardened.

In the case of the new toothed pulley bore, the roughness parameters are shown in Table 1.

Table 1. Roughness parameters

| Roughness parameter | New toothed pulley bore | Worn toothed pulley bore | Crankshaft journal |
|---|---|---|---|
| $R_a$ [μm] | 0.31 ±0.04 | 0.39 ±0.04 | 0.62 ±0.09 |
| $R_{aeq}$ [μm] | 0.93 | 1.01 | |
| $R_z$ [μm] | 2.33 ±0.22 | 2.78 ±0.27 | 4.72 ±0.87 |
| $R_{zeq}$ [μm] | 7.05 | 7.5 | |
| $S_m$ [μm] | 56.34 ±7.21 | 45.56 ±5.07 | 78.31 ±7.19 |
| $S_{meq}$ [μm] | 134.55 | 123.88 | |
| $R_p$ [μm] | 1.17 | 1.39 | 2.36 |
| $R_{peq}$ [μm] | 3.525 | 3.75 | |
| $R_v$ [μm] | 1.40 | 1.67 | 2.832 |
| $R_{veq}$ [μm] | 4.23 | 4.5 | |
| b [-] | 0.83 | 0.80 | 0.83 |
| $b_{eq}$ [-] | 2.76 | 2.66 | |
| ν [-] | 2.76 | 2.56 | 2.81 |
| $\nu_{eq}$ [-] | 5.56 | 5.37 | |
| $\Delta_K$ [-] | 0.011 | 0.035 | 0.021 |
| $\Delta_{Keq}$ [-] | 0.013 | 0.020 | |
| r [μm] | 136.20 | 51.59 | 143.19 |
| $r_{eq}$ [μm] | 274.30 | 187.16 | |

For the new toothed pulley bore, the roughness parameter $R_a$ was close to that for the lapping samples used for friction tests described in [25]. The roughness parameter $R_z$ was 30% lower than the corresponding one used during friction tests described in [25]. The Kombalov complex roughness parameter $\Delta_K$ was is twice as great as the corresponding one used during friction tests described in [25].

### 4.2. The contact pressure in the contact zone

The obtained values of the contact pressure in the contact zone between the crankshaft journal and the toothed pulley bore were presented in Table 2. Contact pressure values for the new shrink-fitted joint vary between 47.73 and 107.84 MPa, while after disassembling, followed by assembling via pressure-fitting of mating components, such values can vary between 24.04 and 87.15 MPa. A decrease in interference from 2.31-fold to 5.21-fold accompanied it.

Table 2. Contact pressure in the contact zone between the crankshaft journal and the toothed pulley bore

| Surfaces state | Sum of smoothing dimensions $G_1 + G_2$ | $p_s$ for $\Delta_{min}$ = 0.027 mm | $p_s/HB$ | $p_s$ for $\Delta_{max}$ = 0.061 mm | $p_s$ /HB |
|---|---|---|---|---|---|
| [-] | [mm] | [MPa] | [-] | [MPa] | [-] |
| New | 0 | 47.73 | 0.195 | 107.84 | 0.110 |
| Worn | 0.0117 | 27.04 | 0.440 | 87.15 | 0.356 |

As all values of the $p_s/HB$ ratio (Table 2) exceeded the value of 0.0625, this indicated that in the contact zone conditions for saturated plastic contact can occur. Therefore, the friction coefficient values calculated from the formula (2) seem to be close to reality.

### 4.3. The penetration depth and the friction coefficient in the contact zone analyzed

For the softer surface of the crankshaft journal, the obtained values of the penetration depth h, the corresponding coefficient k, and the friction coefficient μ in the contact zone are presented in Table 3. For the case of plastic, saturated contact values of the friction coefficient are higher by an order of magnitude compared to those of elastic stress in the contact zone. The calculated values of the friction coefficient for the plastic saturation conditions differ from each other by up to 10%. In the case of new surfaces of the toothed pulley bore and crankshaft journal, the values of the friction coefficient calculated from the formula (1) are close to those obtained during friction tests described in [25] for the mating lapped plates. For the worn surfaces of the toothed pulley and the crankshaft journal mating under the contact pressure $p_s$ values close to 90 MPa, the value of the friction coefficient calculated from formula (1) was 50–70% lower than those obtained for the press-fitted joint hub/shaft made of similar materials and close contact pressure described in [54]. The penetration depth h was twice as low as the corresponding one for the case of the mentioned press-fitted joint described in [54].

Table 3. The values of penetration depth h, corresponding coefficient k and friction coefficient μ for various values of contact pressure, state of mating surfaces and calculation formulas

| Surfaces state | $p_s$ | h | k | μ from formula (1) | μ from formula (2) |
|---|---|---|---|---|---|
| [-] | [MPa] | [mm] | [-] | [-] | [-] |
| New | 47.73 | 0.00183 | 0.916 | 0.069 | 0.441004 |
| | 107.84 | 0.00241 | 0.841 | 0.078 | 0.463792 |
| Worn | 27.04 | 0.00165 | 0.942 | 0.076 | 0.437996 |
| | 87.15 | 0.00243 | 0.838 | 0.091 | 0.471623 |

### 4.4. The friction torque carried by the contact zone

The obtained values of the friction torque carried by the contact zone between the crankshaft journal and toothed pulley bore are presented in Table 4.

Table 4. The values of the friction torque carried by the contact zone between the crankshaft journal and toothed pulley bore for various values of contact pressure, state of mating surfaces, and calculation formulas

| Surfaces state | $p_s$ | M for μ from formula (1) | M for μ from formula (2) |
|---|---|---|---|
| [-] | [MPa] | [Nm] | [Nm] |
| New | 47.73 | 51.45 | 446.36 |
| | 107.84 | 133.29 | 1060.61 |
| Worn | 27.04 | 32.15 | 251.15 |
| | 87.15 | 127.04 | 871.60 |

All values of torque $M_s$ loading the toothed pulley after wear of its bore surface exceed the values of friction torque M carried by the contact zone in case of plastic saturation conditions. However, the presence of oxides, impurities, and engine oil droplets introduced into the contact zone by way of the oil mist present inside the engine block can reduce the friction coefficient in this contact zone. Therefore, especially in conditions of reduced interference between the toothed pulley and the crankshaft journal and in the case of sudden changes in the torque loading the crankshaft, it could occur displacement of the toothed pulley about the crankshaft journal, leading to sudden changes in

the valve timing, incorrect combustion process in the engine cylinders and, as a result, engine failure.

## 5. Summary and conclusions

The analysis of the toothed pulley shrink-fitted to the crankshaft journal was carried out, and the following conclusions can be formulated:

1. The obtained results indicated that disassembling the toothed pulley from the crankshaft journal, followed by their assembly via press-fitting, can significantly weaken the interference between them. It is therefore better to ensure a safer connection between the crankshaft journal and the toothed pulley mounted on it by using a keyed or shaped (splined, elliptical, or other) connection instead of a friction connection.
2. The weakened interface was accompanied by a decrease in contact pressure in the contact zone. The calculated values of contact pressure indicated the occurrence of plastic saturation in the contact zone. In tight friction joints where there is a risk of mutual movement of elements, it is better to use a harder journal and a softer hub or similar hardness of both instead of a softer journal cooperating with a hard hub. The role of ensuring proper quality control of the obtained hardness of the cooperating surfaces is also important.
3. Values of the friction coefficient are higher by an order of magnitude compared to the elastic stress in the contact zone. The calculated values of the friction coefficient for the plastic saturation conditions differ from each other by up to 10%. The coefficient of friction in a tight friction joint depends on many factors, and it is critical to select the optimal initial roughness values in the shrink joint to increase its load transfer efficiency. Such optimization can be carried out experimentally or numerically, but on a complicated and ultimately expensive model that takes into account the elastic-plastic interactions between the vertices of real cooperating surfaces, their surface distributions of profile parameters [58, 75] and their fractal nature [6], the presence of impurities and possibly lubricant particles between the mating surfaces [58]. The use of various artificial Intelligence (AI) tools [4, 56, 69] may be beneficial in such an area.
4. Although all values of torque $M_s$ loading the toothed pulley after wear of its bore surface exceed values of friction torque M carries by the contact zone under plastic saturation conditions, it could occur displacement of the toothed pulley about the crankshaft journal can occur due to possible changes of the friction coefficient in the contact zone.
5. The friction coefficient values can be lowered due to the presence of oxides, impurities, and engine oil droplets introduced into the contact zone by way of the oil mist present inside the engine block.
6. For the assumed value of the interference for the shrink-fitted joint between the toothed pulley and the crankshaft journal, the risk of their mutual displacements cannot be ruled out, especially in the case of sudden changes in the engine torque. Reducing the initial value of this interference will lower the contact pressure value and increase the risk of the mentioned displacements.
7. A press-fit connection should not replace any shrink joint after disassembly. Still, the journal should be re-prepared by applying a repair layer, e.g. via hard steel wire surfacing, followed by grinding and lapping, and re-associated with the new hub by making a shrink joint. The crankshaft journals can also be repaired by other methods like surfacing and spraying, applied by means of electric arc, gas-flame, detonation, and plasma (induction and plasma-arc) methods [57, 61].

## Nomenclature

| | |
|---|---|
| CAI | controlled auto-ignition |
| CI | compression ignition |
| DOHC | double overhead camshaft |
| HCCI | homogeneous charge compression ignition |
| ICE | internal combustion engine |
| OHC | overhead camshaft |
| OHV | overhead valve |
| SI | spark ignition |
| SOHC | single overhead camshaft |
| VVT | variable valve timing |

## Bibliography


[1] Automobile-Catalog. Horsepower/Torque Curve for 2008 Kia CeeD 1.4 EX (man. 5) (model for Europe). Detailed engine characteristics. 2024.

[2] Baker B. Why size and strength matters with pushrods. EngineBuilder. 2019.

[3] Bassey M, Ikpe A, David V. Failure analysis of vehicular camshaft component with variable materials subjected to multi-translated non-proportional loading conditions in its duty cycle. Dans Buenos Aires: Ejons International Journal on Mathematics, Engineering & Natural Sciences. 2023: 82-100.

[4] Batu T, Lemu HG, Shimels H. Application of artificial intelligence for surface roughness prediction of additively manufactured components. Materials. 2023;16(18):6266. https://doi.org/10.3390/ma16186266

[5] Booker JD, Truman CE. Measuring the coefficient of friction for use in shrink-fit calculations. Exp Tech. 2011;35(2): 7-13. https://doi.org/10.1111/j.1747-1567.2009.00593.x

[6] Borodich FM, Gao Z, Jin X. Fractal models in tribology: a critical review. Friction. 2025;13(4):9440945. https://doi.org/10.26599/FRICT.2025.9440945

[7] Browns Automotive. Common causes of timing belt failure. 2023.

[8] Busch M. Structural stability of nonlinear valve train systems in automotive engines. PAMM. 2017;17(1):367-368. https://doi.org/10.1002/pamm.201710153

[9] Calabretta M, Cacciatore D, Carden P. Valvetrain friction – modeling, analysis and measurement of a high performance engine valvetrain system. SAE Int J Engines. 2010;3(2): 72-84. https://doi.org/10.4271/2010-01-1492

[10] Chandiok P, Poonia S, Kundu S, Bharti AK. Hydraulic lash adjuster dynamic behavior prediction using multibody dynamic simulation and co-relation with testing to improve valve train design robustness. SAE Technical Paper 2024-28-0184. 2024. https://doi.org/10.4271/2024-28-0184
[11] Cieślik W, Szwajca F, Wisłocki K. Reverse engineering of research engine cylinder-head. Combustion Engines. 2022; 189(2):73-82. https://doi.org/10.19206/CE-143481
[12] Colin F. Timing belt failure: what causes it? Bolton Engineering Products (BEP) Ltd. 2023.
[13] Domek G, Kołodziej A, Dudziak M, Woźniak T. Identification of the quality of timing belt pulleys. Procedia Eng. 2017; 177:275-280. https://doi.org/10.1016/j.proeng.2017.02.224
[14] Domek G, Kołodziej A, Wilczyński M. Modelling of wear out of timing belt's pulley. IOP Conf Ser Mater Sci Eng. 2020;776(1):012069. https://doi.org/10.1088/1757-899X/776/1/012069
[15] Everlasting Valve Company. What are the types of valve trains used in engines? 2024.
[16] Gates TechZone. The VVT system and the solenoid valve. 2021.
[17] Ghazal OHM, Dado MSH. Gear drive mechanism for continuous variable valve timing of IC engines. Engineering. 2013;5(3):245-250. https://doi.org/10.4236/eng.2013.53035
[18] GSC Power Division. Common causes of camshaft failure. 2025.
[19] HOT ROD Staff. The wrong length pushrod can cost your engine power and performance. MotorTrend 2018.
[20] Howlett M, Ausserhofer N, Schoeffmann W, Truffinet C, Zurk A. Chain versus belt – system comparison of future timing drives. Int J Automot Eng. 2016;7(4):135-141. https://doi.org/10.20485/jsaeijae.7.4_135
[21] Hunicz J, Gęca M. An investigation of supercharged CAI engine with internal gas recirculation and direct gasoline injection. Combustion Engines. 2012;150(3):63-71. https://doi.org/10.19206/CE-117032
[22] Hunicz J, Gęca M. Experimental and modeling study of the gasoline HCCI engine with internal gas recirculation. Combustion Engines. 2013;152(1):3-9. https://doi.org/10.19206/CE-117008
[23] Hunicz J, Niewczas A, Kordos P. A research into a gasoline HCCI engine. Combustion Engines. 2010;140(1):3-13. https://doi.org/10.19206/CE-117154
[24] Innova R&D Department. Common symptoms of a faulty variable valve timing (VVT) solenoid. 2024.
[25] Ivković B, Djurdjanović M, Stamenković D. The influence of the contact surface roughness on the static friction coefficient. Tribol Ind. 2000;22(3-4):41-44.
[26] Jansons E, Lungevics J, Gross KA. Surface roughness measure that best correlates to ease of sliding. Eng Rural Dev. 2016:687-695.
[27] Jelenschi L, Cofaru C, Sandu G. Determining the influence of oil temperature on valve rotation for a direct acting valve train. Ann ORADEA Univ Fascicle Manag Technol Eng. 2012;XXI (XI), 2012/1(1). https://doi.org/10.15660/AUOFMTE.2012-1.2759
[28] Jelenschi L, Cofaru C, Sandu G, Aleonte M. State of the art of engine valve and tappet rotation. Bull Transilv Univ Brasov Ser -Eng Sci. 2011;4(53)(2):19-24.
[29] Jelenschi L, Scutaru ML, Marin M, Cofaru C. Modelling the valvetrain of the car engine to study the effects of valve rotation. Appl Sci. 2022;12(7):3393. https://doi.org/10.3390/app12073393
[30] Kamil M, Rahman MM, A. Bakar R. An integrated model for predicting engine friction losses in internal combustion engines. Int J Automot Mech Eng. 2014;9:1695-1708. https://doi.org/10.15282/ijame.9.2013.19.0141
[31] Keropyan A, Gorbatyuk S. Impact of roughness of interacting surfaces of the wheel-rail pair on the coefficient of friction in their contact area. Procedia Eng. 2016;150:406-410. https://doi.org/10.1016/j.proeng.2016.06.753
[32] Knauder C, Allmaier H, Sander DE, Sams T. Investigations of the friction losses of different engine concepts: part 3: friction reduction potentials and risk assessment at the subassembly level. Lubricants. 2020;8(4):39. https://doi.org/10.3390/lubricants8040039
[33] Li B, Meng F, Li Y, Li T, Mu S. Analysis on failure timing chain system of automobile engine. Run Hua Yu Mi Feng Lubr Eng. 2006;2006(2):52-54.
[34] Lus T. Marine diesel engine valve gear mechanism diagnostics problems. J KONES. 2009;16(4):287-292.
[35] Ma J, Yang L, Song L, Gao Z, Pang S, Han H. Failure analysis of hydraulic expanding assembled camshafts using BP neural network and failure tree theory. Metals. 2022; 12(10):1639. https://doi.org/10.3390/met12101639
[36] Madej J, Śliwka M. Analysis of interference-fit joints. Appl Sci. 2021;11(23):11428. https://doi.org/10.3390/app112311428
[37] Meerkamm H. Schaeffler Technical Pocket Guide. 1st ed. Herzogenaurach, Germany: Schaeffler Technologies GmbH & Co. KG; 2014:432-433.
[38] Mendeleev VYa. Empirical relations for height and spacing parameters of surface roughness. Meas Tech. 2003;46(7): 662-666. https://doi.org/10.1023/A:1025886817541
[39] Mitianiec W, Bac G. Camless hydraulic valve timing system in combustion engines. Combustion Engines. 2011;146(3): 28-37. https://doi.org/10.19206/CE-117089
[40] Morehouse D, Porter J, Hiltz J, Brauss M. Diesel engine valve failures. Virginia Beach, Virginia 2002.
[41] Mukhacheva TL, Kalinina TM, Kusmanov SA. Evaluation of tribotechnical properties of modified surfaces after plasma electrolytic treatment. J Phys Conf Ser. 2021; 2144(1): 012031. https://doi.org/10.1088/1742-6596/2144/1/012031
[42] NEWAY. Common Failures of Automotive Camshafts. News. 2023.
[43] Nowicki B. Geometric structure: surface roughness and waviness/Struktura geometryczna: chropowatość i falistość powierzchni. Wydawnictwa Naukowo-Techniczne, Warszawa 1991.
[44] Patel SV, Pawar SG. Failure analysis of exhaust valve spring of C.I. engine. Int J Eng Res Technol IJERT. 2013; 2(3):1-4.
[45] QuantiServ. Heat Treatment (Annealing). 2025.
[46] Raghuwanshi NK, Pandey A, Mandloi RK. Failure analysis of internal combustion engine valves: a review. Int J Innov Res Sci Eng Technol. 2012;1(2):173-181.
[47] Roodnik T. Literature review on stabilizing high speed valve- and drivetrain concepts for racing applications. [MSc]. University of Twente 2016.
[48] Rostek E, Babiak M, Wróblewski E. The influence of oil pressure in the engine lubrication system on friction losses. Procedia Eng. 2017;192:771-776. https://doi.org/10.1016/j.proeng.2017.06.133
[49] Saleh A, Chaichan M. The effect of variable valve timing on SIE performance and emissions. Int J Sci Eng Res. 2015; 6(8):173-179.
[50] Siczek K. The analysis of operating conditions for valves actuated by camless coupled drive. Combustion Engines. 2009;137(2):93-108. https://doi.org/10.19206/CE-117186
[51] Smigins R, Amatnieks K, Birkavs A, Górski K, Kryshtopa S. Studies on engine oil degradation characteristics in a field test with passenger cars. Energies. 2023;16(24):7955. https://doi.org/10.3390/en16247955

[52] Soffritti C, Merlin M, Vazquez R, Fortini A, Garagnani GL. Failure analysis of worn valve train components of a four-cylinder diesel engine. Eng Fail Anal. 2018;92:528-538. https://doi.org/10.1016/j.engfailanal.2018.06.022
[53] Spinache E, Trandafir A, Diaconu M, Ozuna G, Wozniak M, Kubiak P et al. The effect of $SiO_2$ nanoparticles content in engine oil on tribological properties of valvetrain chain transmission components. Combustion Engines. 2019; 179(4):4-12. https://doi.org/10.19206/CE-2019-401
[54] Stamenkovic D, Milosevic M, Mijajlović M, Banic M. Estimation of the static friction coefficient for press fit joints. J Balk Tribol Assoc. 2011;17(3):341-355.
[55] Steel Express Ltd. Steel Hardness Conversion Table. 2025.
[56] Suman S, Prajapati DK. Predictive modeling of real contact area on rough surfaces using deep artificial neural network. J Tribol. 2025;147(11):111501. https://doi.org/10.1115/1.4068057
[57] Tarasenko B, Dzjasheev AM, Markov V, Zagidullin R, Akhmetshin S, Yakushev A. Method for repairing steel crankshaft joints. Sultanov T (ed.). E3S Web Conf. 2023; 443:04005. https://doi.org/10.1051/e3sconf/202344304005
[58] Taylor RI. Rough surface contact modelling – a review. Lubricants. 2022;10(5):98. https://doi.org/10.3390/lubricants10050098
[59] Technician Academy. What can happen when an engine's variable valve timing fails? 2018.
[60] Thakare AJ, Keche AJ. Optimization of valve-train components for durability analysis by using finite element analysis method. Vijayaraghavan L, Reddy KH, Jameel Basha SM (ed.). Emerging Trends in Mechanical Engineering. Singapore: Springer 2020:11-24. (Lecture Notes in Mechanical Engineering). https://doi.org/10.1007/978-981-32-9931-3_2
[61] Timirâzevskaâ sel′skohozâjstvennaâ akademiâ, Balabanov VI. Analyzing the techniques for restoring crankshafts of automotive vehicles. Agric Eng. 2024;(5):31-38. https://doi.org/10.26897/2687-1149-2024-5-31-38
[62] Trendak M, Czarnigowski J. Influence of oil service life on selected performance parameters of an aircraft piston engine. Combustion Engines. 2023;194(3):78-83. https://doi.org/10.19206/CE-168334
[63] Trodo. Timing belt failure: understanding the damage it can cause. 2023.
[64] Vélez Godiño JA, García MT, Aguilar FJJE, Guerrero DP. Failure analysis of an overhead valve train system in urban buses. Eng Fail Anal. 2019;96:455-467. https://doi.org/10.1016/j.engfailanal.2018.11.003
[65] Wanjari RV, Parshiwanikar TC. Failure of camshaft. Int J Innov Technol Explor Eng IJITEE. 2013;2(6).
[66] Wantuo. 3 Common Bad Rocker Arm Symptoms. 2024.
[67] Woźniak M, Banica CF, Diaconu M, Ozuna G, Jóźwiak P, Siczek K. Investigations on wear and friction in the SI engine valvetrain. Combustion Engines. 2018;175(4):53-64. https://doi.org/10.19206/CE-2018-408
[68] Xin Q, Pinzon CF. Improving the environmental performance of heavy-duty vehicles and engines: particular technologies. Alternative Fuels and Advanced Vehicle Technologies for Improved Environmental Performance. Elsevier 2014:279-369. https://doi.org/10.1533/9780857097422.2.279
[69] Yang H, Zheng H, Zhang T. A review of artificial intelligent methods for machined surface roughness prediction. Tribol Int. 2024;199:109935. https://doi.org/10.1016/j.triboint.2024.109935
[70] Yu ZW, Xu XL. Failure analysis of diesel engine rocker arms. Eng Fail Anal. 2006;13(4):598-605. https://doi.org/10.1016/j.engfailanal.2004.12.039
[71] Yu ZW, Xu XL. Failure analysis on diesel-engine valve springs. J Fail Anal Prev. 2009;9(4):329-334. https://doi.org/10.1007/s11668-009-9247-9
[72] Yuan Y, Wang Z, Wang D, Dong L, Li W, Guo Y. Failure investigation of a marine diesel engine timing gear. Eng Fail Anal. 2020;107:104203. https://doi.org/10.1016/j.engfailanal.2019.104203
[73] Zamros MI, Ku PX. Analysis of fatigue characteristics on camshaft using finite element analysis. J Phys Conf Ser. 2022;2222(1):012010. https://doi.org/10.1088/1742-6596/2222/1/012010
[74] Zhao J, Wang JX, Yu C, Tang SQ, Yao J. Influence of radial interference on torque capacity of shrink-fit camshaft. Adv Mech Eng. 2019;11(4):1687814018817640. https://doi.org/10.1177/1687814018817640
[75] Zhou W, Tang Jy, He Yf, Zhu Cc. Modeling of rough surfaces with given roughness parameters. J Cent South Univ. 2017;24(1):127-136. https://doi.org/10.1007/s11771-017-3415-y
[76] Zou D, McCormick HE. Dynamic model and computer simulation of valve train assemblies with hydraulic lash adjuster. SAE Technical Paper 960351. 1996. https://doi.org/10.4271/960351

Krzysztof Siczek, DSc., DEng. – Department of Vehicles and Fundamentals of Machine Design, Lodz University of Technology, Poland.
e-mail: *ks670907@p.lodz.pl*

Adam Rylski, DEng. – Institute of Materials Science and Engineering, Lodz University of Technology, Poland.
e-mail: *adam.rylski@p.lodz.pl*

Marek Woźniak, DEng. – Department of Vehicles and Fundamentals of Machine Design, Lodz University of Technology, Poland.
e-mail: *marek.wozniak.1@p.lodz.pl*

Prof. Wojciech Stachurski, DSc., DEng. – Institute of Machine Tools and Production Engineering, Lodz University of Technology, Poland.
e-mail: *wojciech.stachurski@p.lodz.pl*